Impact of magnesium addition in zinc oxide matrix for enhanced structural, optical, antimicrobial and anticancer properties

Thiruchelvi M.[1], Senthamilselvi M.M.[2] and Venkatraman B.R.[3]*
1. Department of Science, Nagammai Teacher Training Institute, Periyar Centenary Educational Complex, Tiruchirappalli-620 021, Tamil Nadu, INDIA
2. Kamarajar Government Arts College, Thirunelveli-627 859, Tamil Nadu, INDIA
3. PG and Research Department of Chemistry, Thanthai Periyar Government Arts and Science College (Autonomous), Affiliated to Bharathidasan University, Tiruchirappalli-620 023, Tamil Nadu, INDIA
*brvenkatraman@yahoo.com

Abstract

In the present work, low cost, high efficiency and multifunctional inorganic biocidal (antibacterial and anticancer) materials such as ZnO, MgO and MgZnO nanocomposites (NCs) have been developed with a facile precipitation process. XRD studies confirmed that the prepared NCs exhibit hexagonal, face-centered cubic and hexagonal structures respectively. Transmission electron microscopy (TEM) images revealed spherical shaped ZnO, MgO and MgZnO NCs. The elemental (Zn, Mg and O) compositions of the prepared NMs were identified using EDAX spectra. The photoluminescence (PL) spectra of the prepared NMs revealed oxygen vacancies at 487 nm, 500 nm and 524 nm respectively. They correspond to the active free radicals (OH, O_2 and H_2O_2) production and these results were responsible for their biocidal activities.

Furthermore, the biocidal effects of the MgZnO NCs were studied on the human breast cancer cell line and microbes. The cell viability studies proved that MgZnO NCs possess higher anticancer properties than ZnO and MgO NMs. Overall results displayed that the MgZnO NCs exposed better biocidal effects than ZnO and MgO NMs which can be used for biomedical and industrial applications to improve human health conditions.

Keywords: MgZnO nanocomposites, antibacterial activity, anticancer activity, inorganic biocidal materials.

Introduction

Inorganic biocidal nanomaterials play potentially vital role for disease control in clinical-based healthcare industries. The drug-resistant bacteria are both gram-positive and gram-negative having impact on clinical changes in the healthcare industries[13,15]. They have increased day by day becoming prevalent among the various hospital-acquired infections[30]. People are affected worldwide by gram-positive and gram-negative bacteria infections through *Staphylococcus aureus (S. aureus)* and *Klebsiella pneumoniae (K. pneumonia)* bacteria. They cause severe infections for human system such as respiratory (breathing) tract to cause pneumonia and bloodstream infection. Water and food contaminations cause the most severe dysentery because of potent and deadly Shiga toxin from *S. dysenteriae*.

E. coli bacterial strain may also cause severe anemia or kidney failure. *P. Vulgaris* strain affected wound infections and urinary tract infections[22]. Worldwide, cancer is one of the essential human life-threatening diseases. Cancer treatments like surgery, radiotherapy and chemotherapy methods are having more side effects (nausea, vomiting, stomach cramps, diarrhea). To overcome this problem, it is necessary to develop potential drugs which are highly effective to bacterial and cancer cells, are inexpensive treatment techniques and are non-toxic to human and environmental systems with low-risk factors.[13]

ZnO has exceptional physico-chemical features in semiconducting NM, notably direct bandgap at 3.36eV, binding energy of 60 meV, UV-light absorbance capacity, high stability and less toxicity[16]. Inorganic ZnO NMs are potentially used in photocatalysis, solar cells, gas sensors, paints, wastewater treatment, antibiofilm, antibacterial, anticancer and food packing applications[2,5,18-21,23,27,31]. The photocatalytic abilities of ZnO NMs are promising for the inactivation of microbial and cancer cells. Moreover, antibacterial and anticancer activity of NMs are significantly dependent on their ability to produce reactive oxygen species (ROS)[15]. This is due to their small size, large surface areas, increase in oxygen vacancies and the diffusion ability of the reactant molecules and the release of active ions[9,17].

The size of the material becomes smaller and the bandgap becomes larger, this changes the optical and electrical properties of the material, making it suitable for new biomedical, industrial applications. Among them, the widely accepted method to modify optical and biocidal properties of the semiconductor is the addition of impurity atoms, or doping[9]. MgO is an essential biocompatible, non-toxic and safe inorganic material. However, MgO NMs revealed the unique biocidal property owing to active free oxygen radicals in the aqueous solution[25]. Moreover, cellular macromolecules (Protein, DNA and lipids) are damaged by ROS including (O_2, H_2O_2 and OH^-) and leading to microbial cell and center cells losing viability[13].

A low annealing temperature of 100°C provided the highest antibacterial activity against *S. aureus* and *E. coli* strains[16]. Mg-doped ZnO NMs have better antibacterial potential in

visible-light treatment[10]. MgZnO NPs exhibited excellent selective killing of nasopharyngeal carcinoma cells and cervical cancer cells with minimal toxicity to normal fibroblast cells (L929)[7].

In the present investigation, the ZnO, MgO and MgZnO NCs were successfully developed through a simple precipitation process. The results of the NCs were characterized for their structural, optical, antibacterial and anticancer properties. Mainly, MgO substitution of ZnO NCs biocidal properties has improved by the zone of inhibition and cell viability compared to the ZnO and MgO NMs.

Material and Methods

Materials: Zinc (II) nitrate hexahydrate [$Zn(NO_3)_2$. $6H_2O$], magnesium nitrate hexahydrate [$Mg(NO_3)_2$. $6H_2O$] and sodium hydroxide (NaOH) were purchased from Sigma Aldrich.

Synthesis: The ZnO, MgO and MgZnO NCs were fabricated by precipitation method. In each 250 mL beaker, 0.1M of $Zn(NO_3)_2$. $6H_2O$ and 0.1M $Mg(NO_3)_2$. $6H_2O$ solutes were dissolved in distilled water under constant stirring for 15 min. 0.8 M of NaOH solution was also added dropwise to the zinc nitrate and magnesium nitrate solutions separately. Both solutions yielded a white residue that was agitated for 4 h at an optimum temperature of 60ºC. ZnO and MgO residues were then washed multiple times with deionized water and ethanol and then dried at 120°C. They were then annealed for 5 h at 700ºC.

Synthesis of MgZnO NCs: 0.030M of $Mg(NO_3)_2$. $6H_2O$ solution was mixed into 0.070M of the zinc nitrate solution. Then, 0.8 M of NaOH solution was added dropwise to homogeneous Mg/Zn nitrate solution to form a white residue. Subsequently, the same procedure was followed for ZnO NPs.

Performance of antimicrobial activity: Antibacterial activity targets were against microorganisms gram-positive (*Staphylococcus aureus, Streptococcus pneumonia* and *Bacillus Subtilis*) and gram-negative (*Klebsiella pneumoniae, Escherichia coli, Shigella dysenteriae, Vibrio cholerae, Pseudomonas aeruginosa and Proteus vulgaris*) bacterial strains and *Candida albicans* fungal strains via the well diffusion method. In the present work, bacterial and fungal pathogens were separately mopped on sterile Muller Hinton agar and potato dextrose agar media in isolated Petri disks. The experienced antimicrobial performance was ZnO, MgO and MgZnO NCs at 1mg/mL dispersed in a 5% sterilized DMSO solution. Furthermore, testing Petri plates were incubated overnight at 37°C and the zone of inhibition levels was measured after 24h. The standard antibiotic amoxicillin (30 µg) was used as a positive control. Assays were carried out in triplicate.

Cell culture maintenance: Breast cancer MDA-MB-231 and normal fibroblast L929 cell lines were procured from the cell repository of the National Centre for Cell Sciences (NCCS), Pune, India. Dulbecco`s modified eagle media (DMEM) were used to maintain the cell line, supplemented with 10% Fetal Bovine Serum (FBS). Penicillin (100 U/mL) and streptomycin (100 µg/mL) were added to the medium to prevent bacterial contamination. The medium with cell lines was maintained in a humidified environment with 5% CO_2 at 37°C.

Performance of MTT assay: Cell viability assay, MDA-MB-231 and L929 viable cells were harvested and counted using hemocytometer diluted in DMEM medium. A density of 1 × 104 cells/mL was seeded in 96 well plates for each well and incubated for 24 h to allow attachment. After MDA, MB-231 was treated with control and different concentrations of ZnO, MgO and MgZnO NCs 2.5 to 15 µg/mL were applied to each well. MDA-MB-231 cells were incubated at 37°C in humidified 95% air and 5% CO_2 incubator for 24 h. After incubation, the drug-containing cells wash with a fresh culture medium and the MTT (5 mg/mL in PBS) dye was added to each well followed by incubation for another 4 h at 37°C. The purple precipitated formazan formed was dissolved in 100 µL of concentrated DMSO and the cell viability was absorbance measured at 540 nm using a multi-well plate reader. The results were expressed at the percentage of stable cells with respect to the control. The half maximal inhibitory concentration (IC_{50}) values were calculated and the optimum doses were analyzed at different time periods.

Characterization techniques: The ZnO, MgO and MgZnO NCs were characterized by an X-ray diffractometer (model: X'PERT PRO PANalytical) instrument. The TEM analysis was carried out by instrument Tecnai F20 model operated at an accelerating voltage of 200 kV. The samples were analyzed by EDAX (model: ULTRA 55). The FTIR spectra were recorded in the range of 400-4000 cm^{-1} by using a Perkin-Elmer spectrometer. The PL spectrum of ZnO, MgO and MgZnO NCs was studied in the range between 200 and 800nm by the Jasco V-730 spectrophotometer.

Results and Discussion

XRD analysis: The XRD patterns of ZnO, MgO and MgZnO NCs are shown in fig. 1. The diffraction peaks present at (2θ) at 31.71°, 34.37°, 36.19°, 47.48°, 56.56°, 62.80°, 66.34°, 68.00° and 69.03° and 36.90°, 42.81°, 62.22°, 74.70° and 78.61°, corresponded to the [(100), (002), (101), (102), (110), (103), (200), (112) and (201)] and [(111), (200), (220), (311) and (222)] (hkl) lattice planes of the hexagonal wurtzite structure and face centre cubic structure for ZnO and MgO NMs, which were confirmed by standard JCPDS data (C. NO: 36-1451 and 89-7746)[11,24].

The MgZnO NCs exhibit hexagonal wurtzite structure and the new phase is located at 42.69° and 62.02° corresponding to the cubic phase MgO as shown in fig 1b.ssss By calculating average crystalline size (D) using Scherrer's relation[26], we get:

$$D = \frac{k\lambda}{\beta_D \cos\theta}$$

The crystalline sizes of ZnO, MgO and MgZnO NCs were observed at 45 nm, 52 nm and 37 nm respectively. The reduction in the crystalline size of MgZnO NCs as compared to the ZnO and MgO NMs is mainly due to the distortion in the host ZnO lattice into the foreign impurity (Mg^{2+} ions).

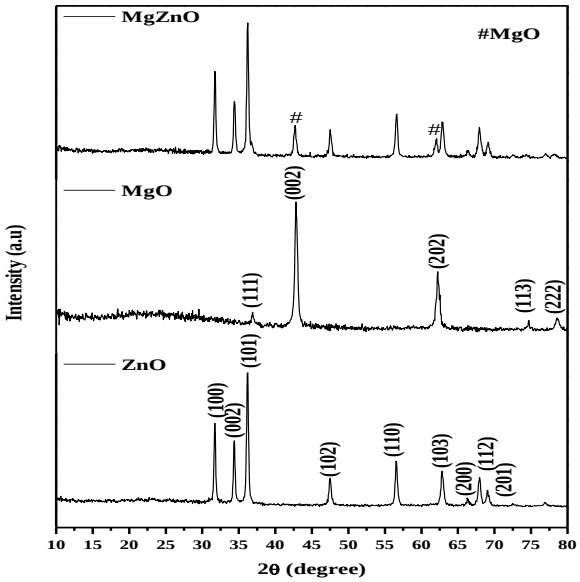

Figure 1a: XRD patterns of ZnO, MgO and MgZnO NCs

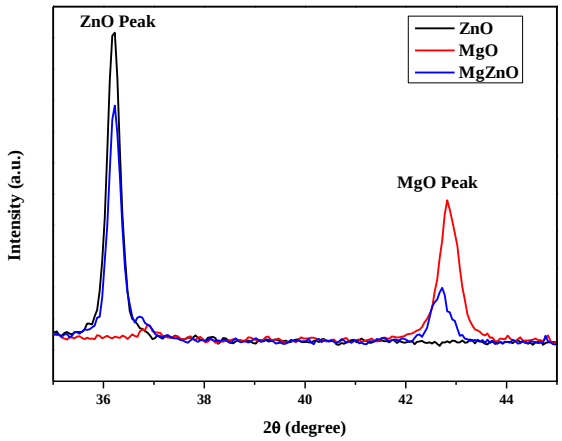

Figure 1b: Enhanced XRD spectra of MgO secondary peaks

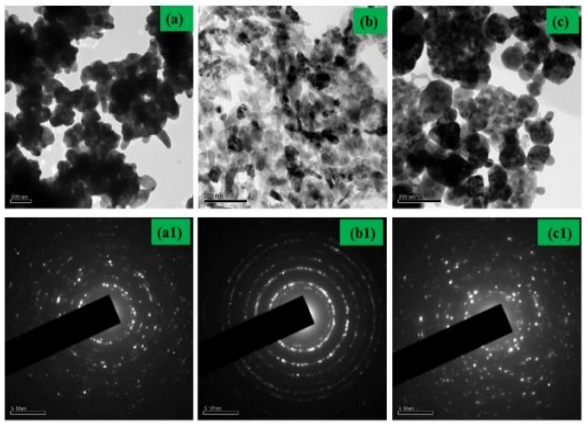

Figure 2: TEM and SEAD patterns of (a-a1) pure ZnO, (b-b1) MgO and (c-c1) MgZnO NCs

Morphological and elemental analysis: Figure 2 (a-c) shows TEM images of the ZnO, MgO and MgZnO NCs calcined at 700°C. The average particle size is observed at approximately 30-60 nm and synthesized ZnO, MgO and MgZnO NCs exhibit spherical structure. The selected area of the electron diffraction (SAED) pattern (Fig. 2 a1-c1) confirms the formation of the ZnO, MgO and MgZnO NCs hexagonal, cubic and hexagonal crystal structures analysis matching with XRD analysis. The elemental of ZnO, MgO and MgZnO NCs was carried out using EDAX analysis as shown in fig. 3a-c. It clearly shows that the amounts of Zn, Mg and O present in the ZnO, MgO and MgZnO NCs as demonstrated in fig. 3. The chemical compositions of (Zn, Cu and O), (Mg, Cu and O) and (Mg, Cu, Zn and O) were found to be (72.24%, 16.33% and 11.43%), (58.99%, 9.92% and 36.18%) and (15.06%, 15.78%, 51.31% 17.86 and 36.18%) respectively.

FTIR spectroscopic analysis: FTIR spectroscopic analysis of ZnO, MgO, MgZnO NCs is shown in fig. 4. The carboxylate and hydroxyl impurities were detected in the 3700-3400 cm^{-1} range[12].The broad O–H stretching modes were 3448, 3449 and 3442$cm^{-1}$for ZnO, MgO and MgZnO NCs which correspond to the hydroxyl group. Symmetric and asymmetric C-H peaks are located[3] at 2852, 2863 and 2853 cm^{-1} and 2922, 2923 and 2930 cm^{-1}. The symmetric C=O bands are observed at 1462cm^{-1} for ZnO NMs. The band at 1435cm^{-1} is attributed to the Mg-O stretching vibration[13]. In the present investigation, both MgO and MgZnO NCs show the Mg-O stretching vibration at 1467 and 1454cm^{-1}. The bands are observed at 876, 867 and 863cm^{-1} due to the C-H out-of-plane bending for the ZnO, MgO and MgZnO NCs. The metal-oxygen (M-O) stretchings such as Zn-O, MgO and Zn-Mg-O stretching bands appear at 420, 425 and 433 cm^{-1} for the ZnO, MgO and MgZnO NCs[13,15] respectively.

PL spectral studies: The PL spectra of ZnO, MgO and MgZnO NCs documented at the excitation wavelength of 325nm are shown in fig. 5. The PL emission peaks of ZnO NMs appeared at 367, 387, 394, 415, 457 and 483 nm. The emission in the UV region is called the near band-edge emission peak appear at 367, 387 and 394 nm generated by the free-exciton recombination[1]. The visible region is known as the deep-level emission, appearing due to the structural defects and impurities in the structures. The violet emission (VE) peak is at 415 nm for natural zinc interstitials (Zn_i) vacancy and the blue emissions at 457 and 483 nm are corresponding to zinc vacancy (V_{Zn})[29]. In MgO NMs, PL emission peaks were observed at 366nm, 394 nm, 413 nm, 449 nm and 500 nm respectively. The NBE was observed at 366 nm and 394 nm. The violet peak located at 413 nm is due to the band-to-band transition. The blue emission is observed at 449 nm corresponding to the electron transition from interstitial defects to oxygen vacancies[25].

The green emission at 500 nm is attributed to the singly ionised charged state of the deficit in MgO causing a radiative switchover of an electron from the deep donor level of Mg interstitial to an acceptor level[6]. However, the PL spectra of MgZnO NCs, peak were observed at 367 nm for the NBE because of the exciton-exciton radiative recombination process. The violet emission peak at 422 nm is attributed to the electron transition from a shallow donor level of the natural zinc interstitials to the top level of the valence band[4]. The blue emission at 459 nm is corresponding to the singly ionized zinc vacancy (V_{Zn}). The green emission peak appears at 524 nm for oxygen vacancies (O_V)[14].

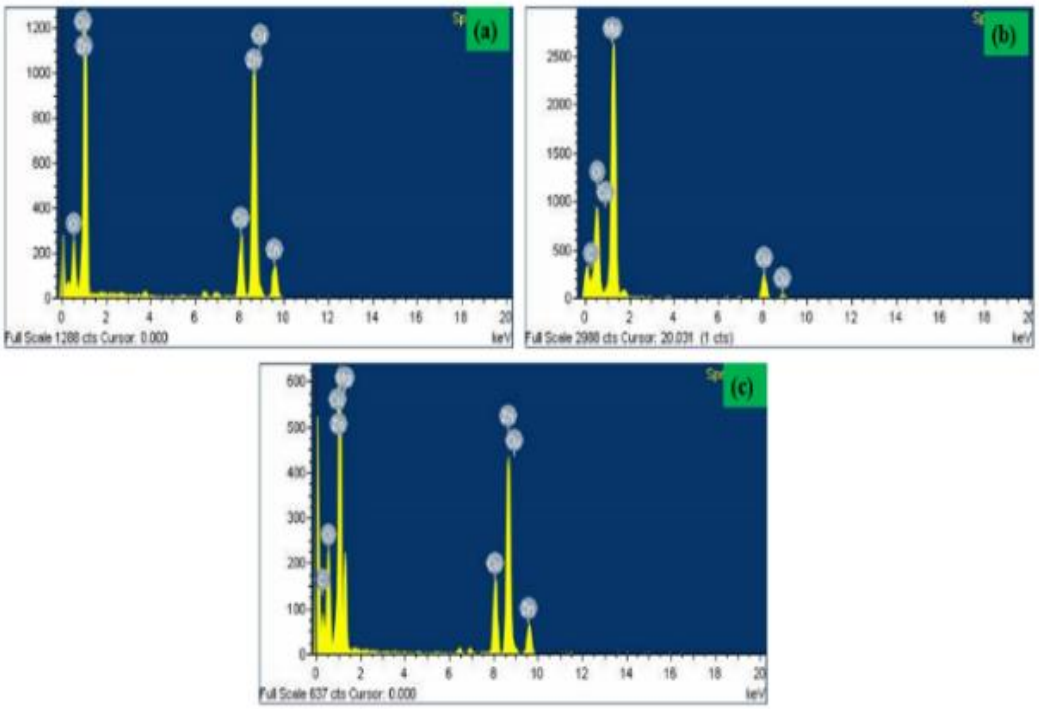

Figure 3: EDAX spectra of (a) ZnO, (b) MgO and (c) MgZnO NCs

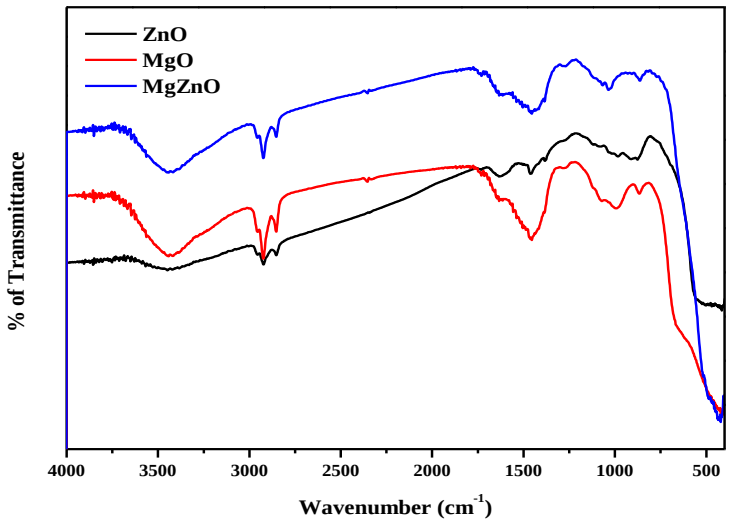

Figure 4: FTIR spectra of ZnO, MgO and MgZnO NCs

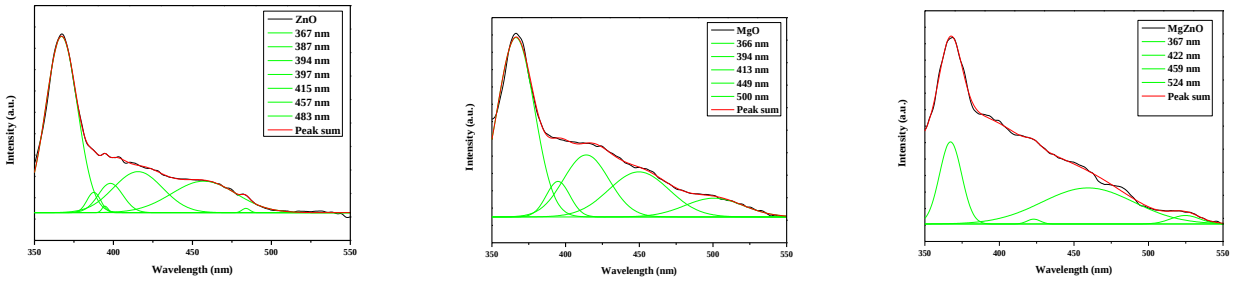

Figure 5: PL spectra of ZnO, MgO and MgZnO NCs

Substitution of Mg atoms into the ZnO lattice surface matrix confirmed these variations in emissions (surface defects). For this reason, MgZnO NCs have a superior potential to produce ROS as well as higher numbers of oxygen vacancies[8]. As a result, MgZnO NCs antibacterial and anticancer properties are based on surface defects. Surface defects such as oxygen vacancy defects are the most important factors in the formation of ROS in this case and they play a major role.

Antimicrobial activity: Antimicrobial activity depends on several parameters such as the membrane and cells which are the essential defensive obstacles to bacterial resistance in the external environment. The lack of a thick peptidoglycan layer in the cell wall and outer membrane that contains lipopolysaccharide, phospholipids and proteins of gram-negative bacteria leads to an increase in bactericidal action on these specimens. In particular, the higher specific surface area to volume ratio for the ZnO NPs caused the generation of more ROS. These ROS are responsible for DNA damage, denaturation of proteins, rupture of enzymes and depletion of antioxidant glutathione levels leading to cell death[28].

From these studies, synthesized ZnO, MgO, MgZnO NCs were tested against gram-positive (*Staphylococcus aureus*, *Streptococcus pneumonia* and *Bacillus Subtilis*) and gram-negative (*Klebsiella pneumoniae*, *Escherichia coli*, *Shigella dysenteriae*, *Vibrio cholerae*, *Pseudomonas aeruginosa* and *Proteus vulgaris*) bacterial strains. *Candida albicans* fungal strain used 1 mg/mL concentration of ZnO, MgO, MgZnO NCs and conventional (10 μg) antibiotics amoxicillin (Fig. 6). ZnO, MgO, MgZnO NCs and amoxicillin are also exhibited. In particular, MgZnO NCs exhibit high antimicrobial effects compared to those of ZnO and MgO NMs. The MgZnO NCs in the tested concentration 1 mg/mL to bacterial and fungal resulted in the range of ZOI of 16–20.

The antimicrobial activity of MgZnO NPs is as follows: When ZnO NPs interact with bacterial cells, they can impact cell membrane integrity, membrane disorganisation and macromolecule structural changes (lipid, DNA and protein). Physical and chemical properties such as larger surface area, uneven ridges on the outer surface and electrostatic attraction (the Zn^{2+} ion is a positive charge and the bacterial cell membrane is a negative charge produced during the interaction of both systems) are observed as the MgZnO NCs enter the cell membrane.

Furthermore, there is an increase in oxygen vacancies, the potential of reactant molecules (impurities) to diffuse and the release of Zn^{2+} ions, all of which can lead to oxidative stress

inside the bacterial cell and the generation of ROS which is highly recommended[14]. The PL emission bands at 483 nm, 500 nm and 524 nm for ZnO, MgO and MgZnO NCs, are corresponding to the oxygen vacancies resulting in a higher number of ROS and another general antibacterial mechanism of the generation of ROS (OH^-, O_2^- and H_2O_2) on the surface matrix of the NMs, when the light-induced oxidative stress in the bacterial cell wall is eventually leading to the death of the cells[14].

Anticancer activity: The anticancer activity of the ZnO, MgO and MgZnO NCs is treated with various concentrations of 2.5−15 µg/mL for the MDA-MB-237 breast cancer cell lines. The anticancer cell death mechanism involved differently, reducing the ZnO NP size, Zn^{2+} ion release and increasing oxygen vacancies. About the cell death, IC_{50} concentration value of 10.15 µg/mL, 11.24 µg/mL and 8.71 µg/mL for ZnO, MgO, MgZnO NCs is well enough to induce 50% cell mortality as shown in fig. 7 (a-c). Among them, MgZnO NCs exhibit a lower dose as compared to the other ZnO and MgO NMs.

The PL studies show several oxygen vacancies (O_V) at 483 nm, 500 nm and 524 nm for ZnO, MgO and MgZnO NCs due to the effects of the high number of ROS generated in the MgZnO NCs[14]. The possible mechanism involved in cancer cell death is: ROS (OH, O_2 and H_2O_2) plays an essential role in eukaryotic cell death by MgZnO NCs. Active free radical molecules contact with the cellular environment; these radicals can oxidize and reduce macromolecules (DNA, lipids and proteins) for significant oxidative stress exerted onto the cells[14].

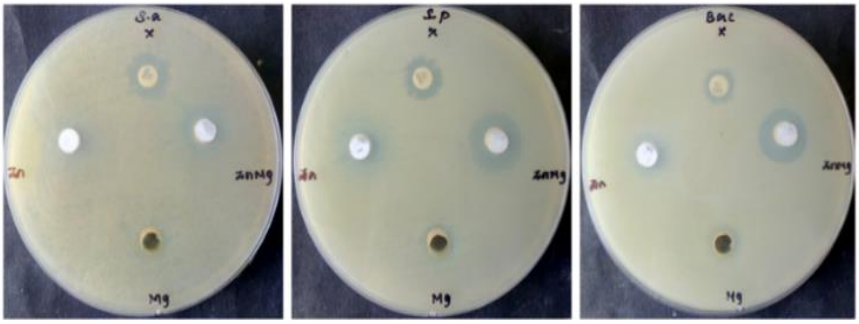

Figure 6a: Zones of inhibition of ZnO, MgO and MgZnO NCs against the investigative gram-positive bacteria

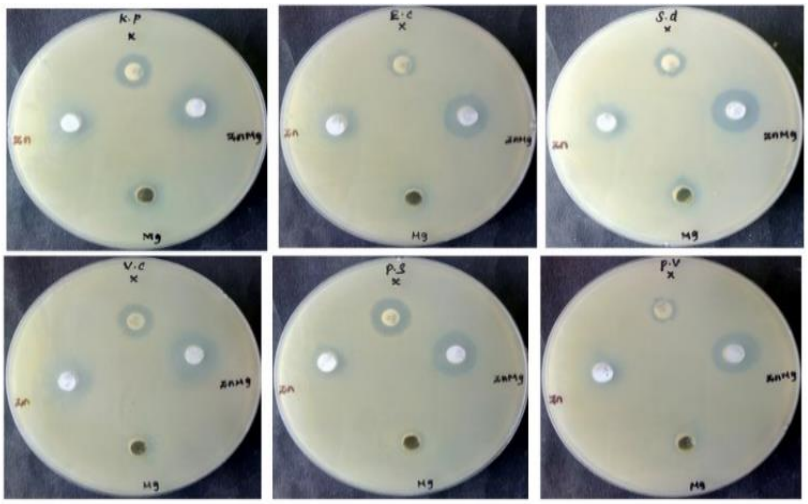

Figure 6b: Zones of inhibition of ZnO, MgO and MgZnO NCs against the investigative gram-negative bacteria

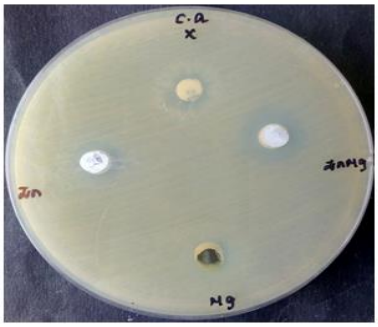

Figure 6c: Zones of inhibition of ZnO, MgO and MgZnO NCs against the investigative fungi

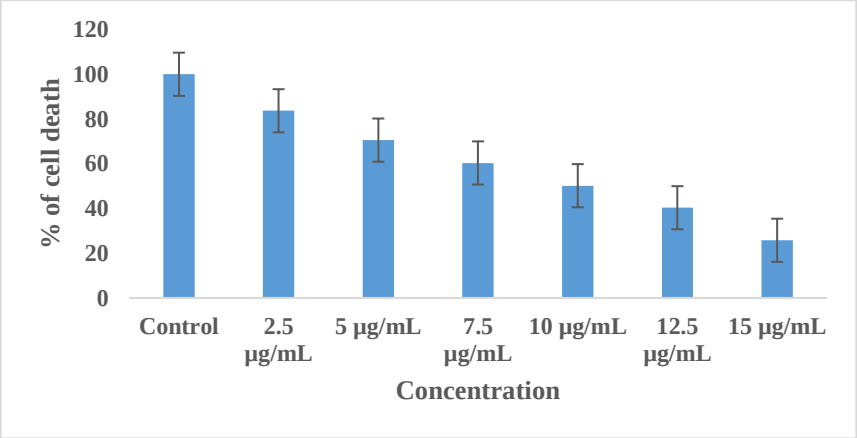

Figure 7a: Anticancer activity of ZnO NMs treated with MDA-MB-237 cancer cell line

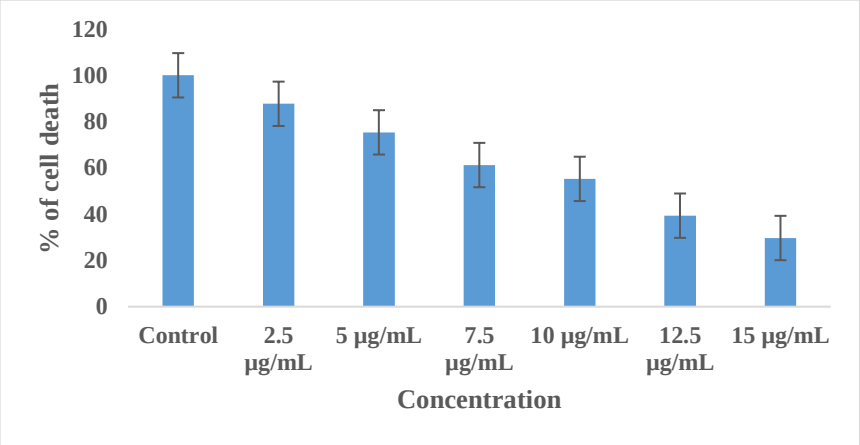

Figure 7b: Anticancer activity of MgO NMs treated with MDA-MB-237 cancer cell line

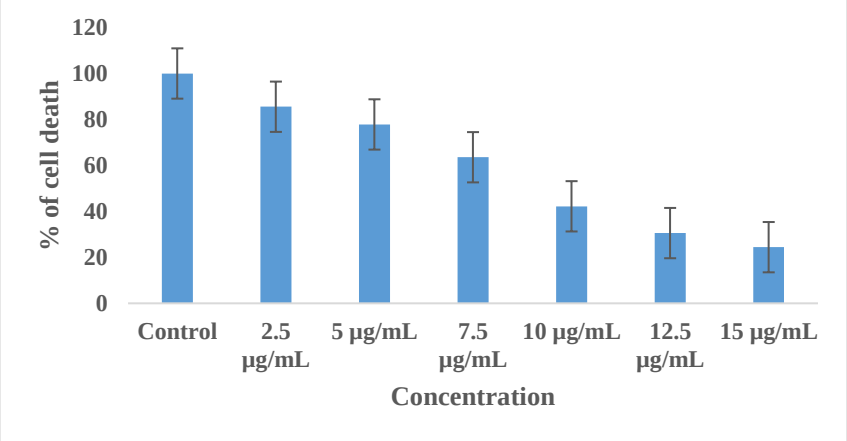

Figure 7c: Anticancer activity of MgZnO NCs treated with MDA-MB-237 cancer cell line

Conclusion

In the present investigation, ZnO, MgO and MgZnO NCs have been synthesized via a precipitation process. The XRD patterns revealed the phase purity of the prepared ZnO, MgO and MgZnO NCs crystallite nature having hexagonal wurtzite, cubic and hexagonal wurtzite structure. From the TEM images, the synthesized NMs formed a spherical structure for ZnO, MgO and MgZnO NCs respectively. Chemical compositions were identified by EDAX analysis. Using the recorded FTIR spectra, the Zn-O, MgO and Zn-Mg-O stretching bands appear at 420, 425 and 433 cm^{-1} for the ZnO, MgO and MgZnO NCs.

The PL studies showed the MgO with ZnO NCs changing the band emission due to zinc vacancies, oxygen vacancies and surface defects. The MgZnO NCs exhibited better antibacterial activity against gram-positive, gram-negative and fungal than that of ZnO and MgO NMs. In addition, the MgZnO NCs exhibited higher cytotoxic activity against human breast cancer cell lines. These findings provide better understanding of MgZnO NCs that can serve as a potential

antimicrobial and anticancer agent in biomedical applications.

References

1. Das S., Das S., Roychowdhury A., Das D. and Sutradhar S., Effect of Gd doping concentration and sintering temperature on structural, optical, dielectric and magnetic properties of hydrothermally synthesized ZnO nanostructure, *Journal of Alloys and Compounds*, **708**, 231-246 **(2017)**

2. Długosz O., Wąsowicz N., Szostak K. and Banach M., Photocatalytic properties of coating materials enriched with bentonite/ZnO/CuO nanocomposite, *Materials Chemistry and Physics*, **260**, 124150 **(2021)**

3. Elemike E.E., Onwudiwe D.C. and Mbonu J.I., Green Synthesis, Structural Characterization and Photocatalytic Activities of Chitosan-ZnO Nano-composite, *Journal of Inorganic and Organometallic Polymers and Materials*, **31(8)**, 3356-3367 **(2021)**

4. Fan X.M., Lian J.S., Zhao L. and Liu Y.H., Single violet luminescence emitted from ZnO films obtained by oxidation of Zn film on quartz glass, *Applied Surface Science*, **252(2)**, 420-424 **(2005)**

5. Gandotra R., Chen Y.R., Murugesan T., Chang T.W., Chang H.Y. and Lin H.N., Highly efficient and morphology dependent antibacterial activities of photocatalytic Cu_xO/ZnO nanocomposites, *Journal of Alloys and Compounds*, **873**, 159769 **(2021)**

6. Garces N.Y., Wang L., Bai L., Giles N.C., Halliburton L.E. and Cantwell G., Role of copper in the green luminescence from ZnO crystals, *Applied Physics Letters*, **81(4)**, 622-624 **(2002)**

7. Gupta J. and Bahadur D., Defect-mediated reactive oxygen species generation in Mg-substituted ZnO nanoparticles: efficient nanomaterials for bacterial inhibition and cancer therapy, *ACS Omega*, **3(3)**, 2956-2965 **(2018)**

8. Hameed A.S.H., Karthikeyan C., Sasikumar S., Kumar V.S., Kumaresan S. and Ravi G., Impact of alkaline metal ions Mg^{2+}, Ca^{2+}, Sr^{2+} and Ba^{2+} on the structural, optical, thermal and antibacterial properties of ZnO nanoparticles prepared by the co-precipitation method, *Journal of Materials Chemistry B*, **43**, 5950-5962 **(2013)**

9. Hameed A.S.H., Karthikeyan C., Ahamed A.P., Thajuddin N., Alharbi N.S., Alharbi S.A. and Ravi G., *In vitro* antibacterial activity of ZnO and Nd doped ZnO nanoparticles against ESBL producing *Escherichia coli* and *Klebsiella pneumoniae*, *Scientific Reports*, **6(1)**, 1-11 **(2016)**

10. Ikram M., Aslam S., Haider A., Naz S., Ul-Hamid A., Shahzadi A., Ikram M., Haider J., Ahmad S.O.A. and Butt A.R., Doping of Mg on ZnO nanorods demonstrated improved photocatalytic degradation and antimicrobial potential with molecular docking analysis, *Nanoscale Research Letters*, **16,** 78 **(2021)**

11. Inbaraj, P. and Prince J.J., Optical and structural properties of Mg doped ZnO thin films by chemical bath deposition method, *Journal of Materials Science: Materials in Electronics*, **29(2)**, 935-943 **(2018)**

12. Karthik K.V., Raghu A.V., Reddy K.R., Ravishankar R., Sangeeta M., Shetti N.P. and Reddy C.V., Green synthesis of Cu-doped ZnO nanoparticles and its application for the photocatalytic degradation of hazardous organic pollutants, *Chemosphere*, **287**, 132081 **(2022)**

13. Karthikeyan C., Sisubalan N., Sridevi M., Varaprasad K., Basha M.H.G., Shucai W. and Sadiku R., Biocidal chitosan-magnesium oxide nanoparticles via a green precipitation process, *Journal of Hazardous Materials*, **411**, 124884 **(2021)**

14. Karthikeyan C., Tharmalingam N., Varaprasad K., Mylonakis E. and Yallapu M.M., Biocidal and biocompatible hybrid nanomaterials from biomolecule chitosan, alginate and ZnO, *Carbohydrate Polymers*, **274**, 118646 **(2021)**

15. Karthikeyan C., Varaprasad K., Venugopal S.K., Shakila S., Venkatraman B.R. and Sadiku R., Biocidal (bacterial and cancer cells) activities of chitosan/CuO nanomaterial, synthesized via a green process, *Carbohydrate Polymers*, **259**, 117762 **(2021)**

16. Kasi G., Viswanathan K. and Seo J., Effect of annealing temperature on the morphology and antibacterial activity of Mg-doped zinc oxide nanorods, *Ceramics International*, **45(3)**, 3230-3238 **(2019)**

17. Kim A., Won Y., Woo K., Kim C.H. and Moon J., Highly transparent low resistance ZnO/Ag nanowire/ZnO composite electrode for thin film solar cells, *ACS Nano*, **7(2)**, 1081-1091 **(2013)**

18. Mousavi-Kouhi S.M., Beyk-Khormizi A., Amiri M.S., Mashreghi M. and Yazdi M.E.T., Silver-zinc oxide nanocomposite: From synthesis to antimicrobial and anticancer properties, *Ceramics International*, **47(15)**, 21490-21497 **(2021)**

19. Pauzi N., Zain N.M., Kutty R.V. and Ramli H., Antibacterial and antibiofilm properties of ZnO nanoparticles synthesis using gum arabic as a potential new generation antibacterial agent, *Materials Today: Proceedings*, **41(1)**, 1-8 **(2021)**

20. Qian C., Yin J., Zhao J., Li X., Wang S., Bai Z. and Jiao T., Facile preparation and highly efficient photodegradation performances of self-assembled Artemia eggshell-ZnO nanocomposites for wastewater treatment, *Colloids and Surfaces A: Physicochemical and Engineering Aspects*, **610,** 125752 **(2021)**

21. Qin W., Yuan Z., Gao H., Zhang R. and Meng F., Perovskite-structured $LaCoO_3$ modified ZnO gas sensor and investigation on its gas sensing mechanism by first principle, *Sensors and Actuators B: Chemical*, **341**, 130015 **(2021)**

22. Rahman M.A., Radhakrishnan R. and Gopalakrishnan R., Structural, optical, magnetic and antibacterial properties of Nd doped NiO nanoparticles prepared by co-precipitation method, *Journal of Alloys and Compounds*, **742**, 421-429 **(2018)**

23. Ramya M., Nideep T.K., Nampoori V.P.N. and Kailasnath M., Solvent assisted evolution and growth mechanism of zero to three dimensional ZnO nanostructures for dye sensitized solar cell application, *Scientific Reports*, **11(1)**, 1-14 **(2021)**

24. Jain Savita M., Manju Vij A. and Thakur A., Impact of annealing on the structural properties of MgO nanoparticles by

XRD analysis and Rietveld refinement, *AIP Conference Proceedings*, **2093(1)**, 020024 **(2019)**

25. Sawai J., Kojima H., Igarashi H., Hashimoto A., Shoji S., Sawaki T., Hakoda A., Kawada E., Kokugan T. and Shimizu M., Antibacterial characteristics of magnesium oxide powder, *World Journal of Microbiology and Biotechnology*, **16(2)**, 187-194 **(2000)**

26. Selvi K.T., Mangai K.A., Priya M. and Sagadevan S., Investigation of the dielectric and impedance properties of ZnO/MgO nanocomposite, *Physica B: Condensed Matter*, **594**, 412355 **(2020)**

27. Sheteiwy M.S., Shaghaleh H., Hamoud Y.A., Holford P., Shao H., Qi W. and Wu T., Zinc oxide nanoparticles: potential effects on soil properties, crop production, food processing and food quality, *Environmental Science and Pollution Research*, **28,** 36942-36966 **(2021)**

28. Sirelkhatim A., Mahmud S., Seeni A., Kaus N.H.M., Ann L.C., Bakhori S.K.M., Hasan H. and Mohamad D., Review on zinc oxide nanoparticles: antibacterial activity and toxicity mechanism, *Nano-Micro Letters*, **7(3)**, 219-242 **(2015)**

29. Stoyanova D., Stambolova I., Blaskov V., Georgieva P., Shipochka M., Zaharieva K., Dimitrov O., Markov P., Dyakova V., Kostova Y., Mladenova R., Tzvetkov G., Boshkova N. and Boshkov N., Modified Approach Using Mentha arvensis in the Synthesis of ZnO Nanoparticles-Textural, Structural and Photocatalytic Properties, *Applied Science*, **12**, 1096 **(2022)**

30. Xia H., Horn J., Piotrowska M.J., Sakowski K., Karch A., Tahir H., Kretzschmar M. and Mikolajczyk R., Effects of incomplete inter-hospital network data on the assessment of transmission dynamics of hospital-acquired infections, *PLoS Computational Biology*, **17(5)**, e1008941 **(2021)**

31. Xu P., Wang P., Wang Q., Wei R., Li Y., Xin Y., Zheng T., Hu L., Wang X. and Zhang G., Facile synthesis of Ag_2O/ZnO/rGO heterojunction with enhanced photocatalytic activity under simulated solar light: Kinetics and mechanism, *Journal of Hazardous Materials*, **403**, 124011 **(2021)**.

(Received 15th March 2022, accepted 21st April 2022)